JOURNAL OF APPLIED PHYSICS **117**, 053101 (2015)

Optical and magneto-optical properties of Au:$Co_{nanoparticles}$ and Co:$Au_{nanoparticles}$ doped magnetoplasmonic systems

D. Martín-Becerra,[1,a)] J. M. García-Martín,[1] Y. Huttel,[2] and G. Armelles[1,b)]
[1]*IMM-Instituto de Microelectrónica de Madrid (CNM-CSIC), Isaac Newton 8, PTM, E-28760 Tres Cantos, Madrid, Spain*
[2]*Instituto de Ciencia de Materiales de Madrid (ICMM-CSIC), c/Sor Juana Inés de la Cruz, 3, 28049 Cantoblanco, Madrid, Spain*

(Received 10 September 2014; accepted 15 January 2015; published online 2 February 2015)

We report a study of Au:Co_{NPs} and Co:Au_{NPs} doped magnetoplasmonic systems. In particular, we analyze the effect of adding different concentrations of Co (or Au) nanoparticles (NPs) in a Au (or Co) matrix on both the optical and magneto-optical constants. Through the use of a simple effective medium model, relevant changes in the optical properties of the Au NPs compared to those of bulk material have been identified. Such effects are not observed in the Co NPs system. However, in both systems, there is an increase of the effective diameter of the NPs as compared to the real diameter that can be due to interface effects surrounding the NPs. Moreover, the magneto-optical constants values of both systems are smaller (in absolute values) than expected, which could also be attributed to interface effects such as hybridization between Au and Co. [http://dx.doi.org/10.1063/1.4906946]

I. INTRODUCTION

Plasmonics is an increasing topic of research, due to the many potential applications in very different areas such as sensing,[1] medicine,[2] or circuitry.[3] Magnetoplasmonics relates the plasmonic behavior with the magnetic field, either modulating the plasmon by applying an external magnetic field or by increasing the magneto-optical (MO) effects by the presence of a plasmon.[4–7] This makes magnetoplasmonics very attractive from an application point of view, since it can conduce to more sensitive sensors[8] and can lead to active plasmonic devices.[9] To reach reasonable magnetoplasmonic effects, however, a material combining appropriate plasmonic properties and MO constants is needed. Those two characteristics are obtained from the dielectric tensor, where the diagonal components (ε_{xx}) are related to the plasmonic response and the non-diagonal ones (ε_{xy}) are the magneto-optical constants. Noble metals have large Re(ε_{xx}), but relatively small absorption Im(ε_{xx}), leading to large plasmon propagation distances. Nevertheless they present very small MO constants. On the other hand, ferromagnetic metals, such as Co, have a not very large Re(ε_{xx}), and are quite absorbent (huge Im(ε_{xx})), which reduces a lot of the propagation distance of the plasmon. Nevertheless, they have large MO constants. There have been several approaches to reach the best magnetoplasmonic system such as noble metal/ferromagnetic metal multilayer structures,[9–12] noble metal/ferromagnetic metal nanocomposite thin films,[13] or noble metal/ferromagnetic dielectric structures.[14–18] Also systems consisting of magnetic nanoparticles (NPs) embedded in a dielectric matrix,[19,20] as well as noble metal-ferromagnetic metal nanostructures in a dielectric matrix have been studied to obtain ferromagnetism and plasmonics together.[21,22] Here, we propose two complementary metallic systems consisting of Co NPs embedded in a Au matrix and vice versa, i.e., Au NPs in an Co matrix (from now Au:Co_{NPs} and Co:Au_{NPs}, respectively). In those two systems, we want to study the improvement of the magnetoplasmonic properties of Au and Co thin films, respectively.

II. NPs DOPED SYSTEMS

The two matrix:NPs doped sets of samples were obtained by sequential deposition of continuous layers of the matrix material (by e-beam evaporation or a Knudsen cell for Co or Au, respectively) and NPs layers (by an ion cluster source, ICS).[23,24] In all cases, the systems were deposited on a silicon substrate covered by a 2 nm thick Ti buffer layer by e-beam evaporation. A first buffer layer of the matrix (6 nm Au or 12 nm Co layer) was deposited in order to have the NPs embedded in a symmetric environment. Subsequently, the NPs generated by an ICS were deposited, followed by the deposition of a matrix layer. The sequential deposition of the NPs layer and the matrix layer was repeated 5 times. Finally, the samples were capped with a final protecting layer to prevent oxidation: the Au:Co_{NPs} samples with a Au layer of 4 nm thick and the Co:Au_{NPs} samples with a 40 nm thick SiO_2 layer. The diameter of the NPs was determined by measuring their height with atomic force microscopy (AFM) in calibration samples (see Fig. 1), using Next-Tip probes[25] and assuming spherical shape for the NPs.[23] Statistics with about 130 NPs in each case allowed the determination of the diameter distributions, which were fitted with a LogNormal function: Co and Au NPs have a mean diameter of 5.1 ± 0.5 nm and 6.5 ± 0.5 nm, respectively. The concentration of NPs was controlled by the deposition time. The deposition rate was 2.9 and 73 NPs/(μm^2 s) for Co NPs and Au NPs, respectively (the small value obtained for Co NPs is mainly due to the decrease of the magnetron efficiency when using magnetic

a)Email: diana.martin@imm.cnm.csic.es
b)Email: gaspar@imm.cnm.csic.es

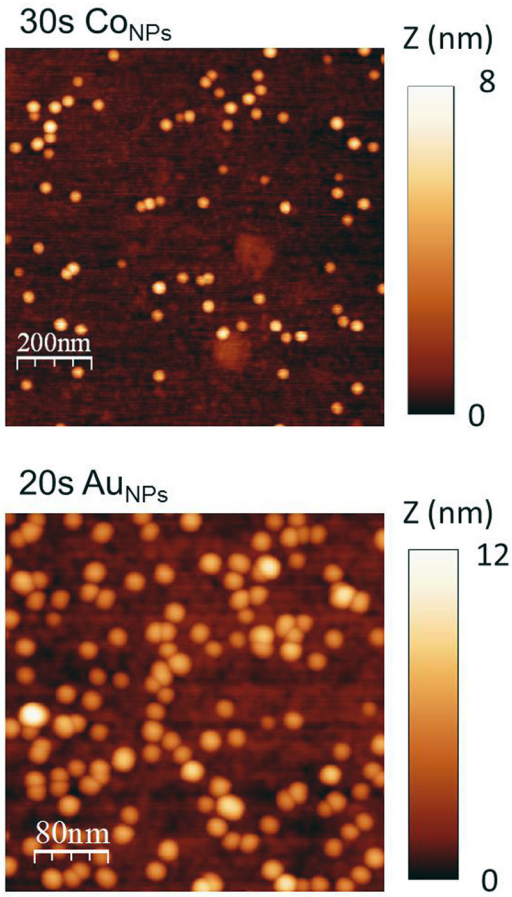

FIG. 1. AFM images of calibration samples of Co_{NPs} with a deposition time of 30 s on a Si substrate (up); and of Au_{NPs} with a deposition time of 20 s on a Si substrate (down).

targets). For the Au:Co_{NPs} set, 0, 144, and 360 s deposition times were used (will appear as Au, t_{Co} and $2.5{\cdot}t_{Co}$, respectively, in the graphics) and for the Co:Au_{NPs} set, deposition times of 0, 20, 50, and 80 s were used (will appear as Co, t_{Au}, $2.5{\cdot}t_{Au}$, and $4{\cdot}t_{Au}$ in the graphics). The NPs concentration are determined by the diameter of the NP and the number of NPs, resulting in NP volume concentrations of 0.4% and 1% for the deposition times of 144 and 360 s of the Au:Co_{NPs} set and of 1.8%, 4.5%, and 7.2% for the deposition times of 20, 50, and 80 s of the Co:Au_{NPs} set. In Fig. 1, we show the AFM images of calibration samples with Co (up) and Au (down) nanoparticles deposited during 30 and 20 s, respectively, on Si substrates. As can be observed, the deposition of the nanoparticles is random like and the NPs are isolated, although for the Au_{NPs} case they seem to be in contact due to the convolution of the measured NPs and the AFM tip. Other studies performed with AFM and TEM have demonstrated that the shape of the NPs is spherical even when they land on the substrate, and that the height measured by AFM is equal to the diameter measured by TEM.[23,24]

III. RESULTS AND DISCUSSION

A. Optical properties

The optical properties of the two systems were obtained from ellipsometry measurements, in the spectral range of 400–1500 nm (0.826–3.1 eV). For the Co:Au_{NPs} set, the optical properties of the 40 nm thick SiO_2 protective layer were obtained from ellipsometry measurements of an equivalent SiO_2 layer deposited on a Si substrate. For both sets, as the equivalent thickness of the coating layer that separates the NPs layers is much shorter than the wavelength of light (6 nm or 12 nm depending on the set), the matrix:NPs structure can be considered as an effective layer, whose thickness is the thickness of the structure: 5×(CoNPs/Au, 34 nm with the capping layer) or 5×(AuNPs/Co, 60 nm). Those thicknesses have been confirmed by combining X-ray reflectivity measurements with the total thickness of the structures measured by AFM in the steps created during the deposition by the shadow of the clips of the sample holder.

Fig. 2 presents the effective dielectric constants of the Au:Co_{NPs} layers. As it can be observed, the real part of the dielectric constant is nearly the same for all the samples, with a slight reduction of the absolute value for higher Co NPs concentrations. The imaginary part however increases as the Co NPs concentration is increased. The graphics at the right side represent the theoretical evolutions of the dielectric constants as a function of the NPs concentration calculated using an effective medium approximation (Maxwell-Garnet[26,27] or Bruggeman[28] that give similar results for the concentrations studied here). In this approximation (hereinafter, called EMA simulation), the whole structure is considered as a homogeneous material of effective dielectric constant ε_{xx}, which depends on the optical constants and on the concentration of the two materials that constitute the system, i.e., Au and Co in our systems. Despite that the evolution with the concentration of Co nanoparticles of the theoretical simulation is similar to the experimental one, the experimental changes are more pronounced than those of the

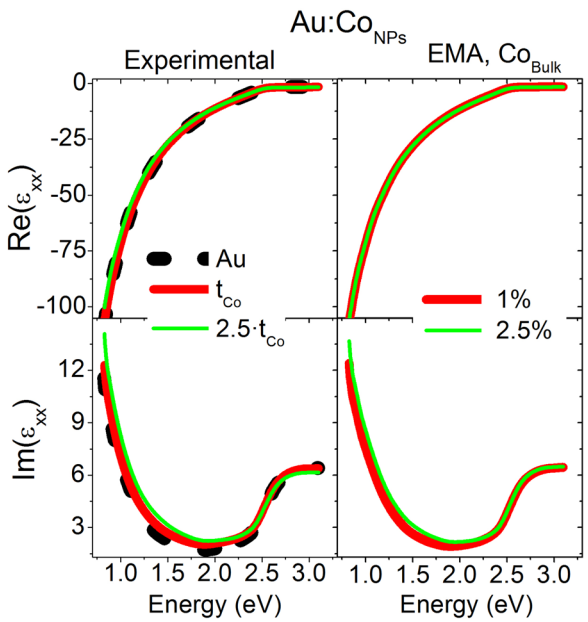

FIG. 2. The left graphics show the experimental optical constants of the Au:Co_{NPs} set. The graphics at the right side display the EMA simulations of the Au:Co_{NPs} system with concentrations according to an effective diameter of 7 nm. The upper graphics show the real part of ε_{xx}, while the lower ones show the imaginary part.

EMA simulations (not shown in the graphic). Such bigger changes can be taken into account if we increase the Co NPs concentration using an effective optical size of the Co NPs different from that obtained by AFM (that would lead thus to different concentrations). The evolution of the optical properties assuming a larger effective diameter is presented in the right graphics of Fig. 2. The results suggest that this effective optical size mimics the changes in the optical properties of the Co NPs region, which could be due to interface effects. In particular, it has been shown that the interface region between metallic nanoparticles and the matrix has different optical properties.[29]

In Fig. 3, we present the dielectric constants of the complementary system, i.e., Co:Au_{NPs} layers. As it can be seen, the real part of the dielectric constant is very similar for all the samples, and displays a decreasing of the absolute value for higher NPs concentrations. The imaginary part decreases as the NPs concentration is increased. As it can be observed at the right side of the figure, the theoretical evolution of the dielectric constants is completely different to the experimental one (contrary to what happened for the Au:Co_{NPs} system). In particular, in the infrared range, the theoretical simulations show an increase of the absolute value of the real part, whereas the experimental values show the opposite behaviour. Moreover, the evolution of the experimental imaginary part is much more pronounced than the theoretical ones with the NPs concentration variation. These results for the Co:Au_{NPs} system strongly suggest that the optical properties of Au NPs are different from the optical properties of bulk material, as could be expected.[30] In particular, the Au NPs of the system should have both an imaginary part of the dielectric constant and an absolute value of the real part lower than those of bulk Au (Fig. 3). In the infrared range (energies <1.9 eV approximately), the main contribution to the optical properties of Au comes from the conduction electrons that can be described using a Drude model

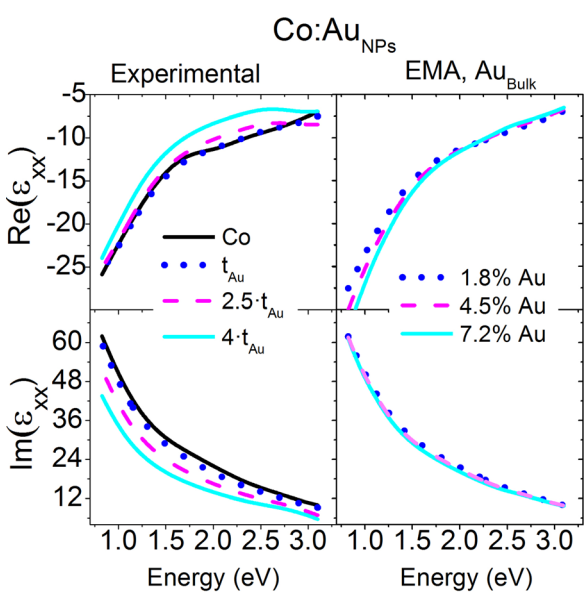

FIG. 3. Experimental optical constants (left) and EMA simulations for the equivalent Au concentrations (right) as a function of the energy for the different Au NPs deposition times. The upper graphs represent the real part of the optical constants, while the lower ones represent the imaginary parts.

$$\varepsilon(\omega) = \varepsilon_\infty - \frac{\omega_p^2}{\omega^2 + i\Gamma\omega}, \tag{1}$$

where ω_p is the plasma frequency ($\omega_p^2 = \frac{ne^2}{m^*\varepsilon_0}$, n being the electron concentration and m* is the effective mass). Γ is the relaxation frequency of the electrons, and ε_∞ can be different from 1 to take into account the interband transitions located at very high energy.

In Fig. 4, we present the experimental optical properties of Au and the free electron contribution to the dielectric constant extracted from (1) for both Au and Co. As it can be observed, in the infrared range the optical properties of Au are determined by the intraband transition (free electron contribution, green curves in Fig. 4), whereas at higher energies the interband transitions start to play a role. On the other hand, both inter and intra band transitions contribute to the dielectric constant of Co. Taking into account that the main component of the system is the metallic Co, which implies that the electrons propagate in both the Au NPs and the Co matrix, we could use as a first approach the Co Drude parameters (that produce the optical constants represented as the purple curve[31]) to simulate the free electrons contribution to the optical properties of the Au NPs, shown as the magenta dotted line of Fig. 4. This gives rise to a reduction of both the imaginary part and the absolute value of the real part of the Au NPs dielectric constant (magenta dotted line).

With these new NPs optical properties, we can calculate the theoretical evolution of the dielectric constants of the Co:Au_{NPs} system as a function of Au NPs concentration that are presented in the left insets of Fig. 5. It can be observed that the theoretical evolution with the Au NPs concentration

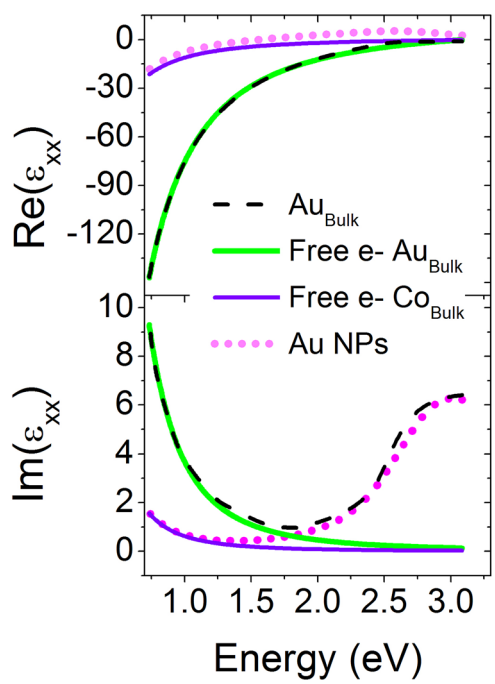

FIG. 4. Optical properties of Au as a function of the energy. The black dashed curves represent the constants of a bulk Au layer, and the thick green curves the theoretical free electron contribution from a Drude model for Au, while the purple line represents the free electron contribution from a Drude model for Co. The magenta dotted curves show the obtained optical constants for the Au NPs.

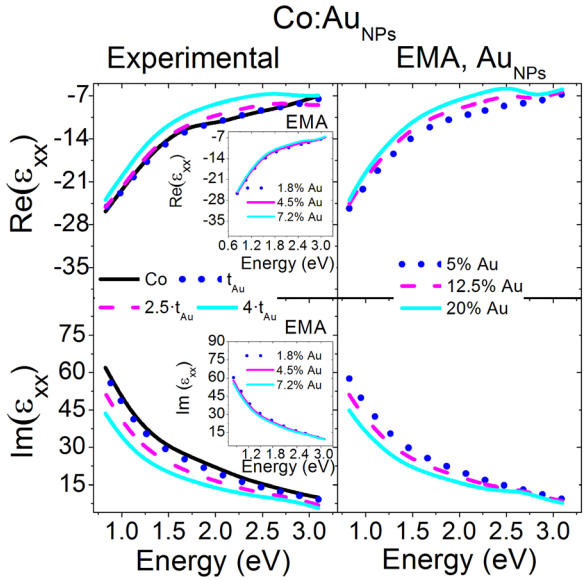

FIG. 5. The insets of the left side represent an EMA simulation for the Co:Au_{NPs} system using the Au NPs dielectric constants (magenta dashed curve), whereas the main graphs of the right are the same EMA simulations performed with concentrations according to an effective NPs diameter of 9 nm. The main graphic of the left side shows the experimental optical constants for the Co:Au_{NPs} set.

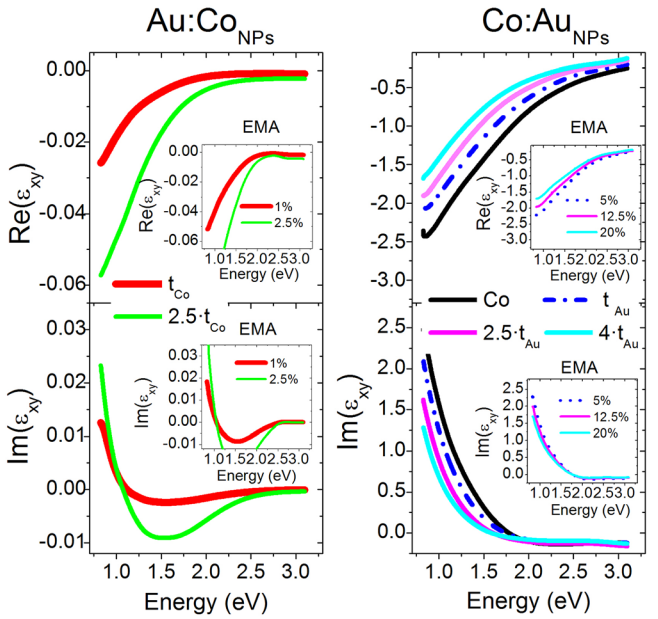

FIG. 6. Experimental (main graphics) and EMA simulations (insets) of the MO constants as a function of the energy for the Au:Co_{NPs} system (left) and for the Co:Au_{NPs} system (right). The upper graphs show the real parts of ε_{xy}, while the lower ones show the imaginary parts.

of both real and imaginary parts is more similar to the experimental one (main graphics of the left side). Nevertheless, the theoretical changes in the imaginary part are still lower than the experimental ones. The changes in the optical properties should not be limited to the Au NPs region, but it may affect Co regions around the NPs. Such effect would increase the effective diameter of the NPs (as also happened in the Co:Au_{NPs} set). In fact, in the graphics at the right side of Fig. 5, we display the evolution of the optical properties that best fit the experimental results, assuming an effective NPs diameter of 9 nm. As it can be observed, these results are almost identical to the experimental ones (graphs of the left side).

B. Magneto-optical properties

The MO constants were obtained from Polar Kerr measurements using the previously obtained optical constants.[5] The measurements of the Polar Kerr Rotation and Ellipticity spectra have been performed at a maximum applied magnetic field of 1.1 T. At this field, the Au:Co_{NPs} set of samples were completely saturated. On the other hand, the Co:Au_{NPs} samples were not completely saturated, since the samples saturate at about 2 T. Therefore, in order to obtain the appropriate MO constants (ε_{xy}), we have multiplied our initial results by the corresponding factor (obtained from hysteresis loops where the samples reached saturation) in order to compensate the fact that the rotation and ellipticity were not obtained in saturation conditions. Fig. 6 displays the MO constants for both systems, Au:Co_{NPs} (left) and Co:Au_{NPs} (right). We present the experimental values as well as the theoretical values of the non-diagonal dielectric constant for the different NPs concentrations calculated using an effective medium approximation as described in Ref. 28. In these simulations, the non-diagonal components of the effective medium ε_{xy} depend on the previously obtained diagonal ones ε_{xx}, and on the optical and MO constants of the materials that constitute the medium; $\varepsilon_{xx,Au}$ and $\varepsilon_{xx,Co}$ and $\varepsilon_{xy,Co}$. The proportion of the two materials and the shape of the NPs (spherical in this manuscript) are also considered.

As it can be observed, for the Au:Co_{NPs} system the absolute values of both real and imaginary parts of the non-diagonal elements of the dielectric tensor increase with the Co NPs concentration, as expected. But the values of the effective dielectric MO constant obtained using the same Co NPs concentration that mimics the evolution of the optical properties are higher than the experimental ones. This difference could be attributed to a reduction of the MO properties in the Co NP region. In particular, it has been shown that at the interface region between Co and Au, strong hybridization occurs between Co and Au atoms.[29,32] This interface region has a MO activity opposite in sign to that of Co,[32] which will lead to an effective decrease (absolute value) of the ε_{xy} with the NPs concentration than the theoretical results presented in Fig. 6. For the Co:Au_{NPs} system, the absolute values of both real and imaginary parts of the non-diagonal dielectric constant decrease as the Au NPs concentration increases. In those calculations, the NPs have no MO activity, the same diameter that reproduces the experimental optical results, and the optical constants are those of the magenta dotted line of Fig. 4. We observe that the calculated reduction of the MO activity with the NPs concentration is not as large as the experimental ones. This agrees with the results from the Au:Co_{NPs} system that suggest the presence of an interface region surrounding the NPs where hybridization between Co and Au takes place.[29,32] In this situation, the interface would also have a MO activity opposite to that of Co.[32]

With this optical and MO characterization, it is desirable to know the properties of these materials for

magnetoplasmonics. This can be done by means of a figure of merit[9,33] that involves both the magneto-optical effect (reflected in the values of the magnetic modulation of the surface plasmon polariton (SPP) wavevector, Δk) and the plasmonic properties (also involved in Δk) such as the propagation distance, L. Therefore, an appropriate magnetoplasmonic material will show large values of the figure of merit, provided it has a large enough propagation distance L to be useful. For the Au:Co_{NPs} system, the SPP propagation distance is almost constant ($L = 16\,\mu m$ at 700 nm), as could be deduced from Fig. 3, since the optical constants were very similar for all the samples of the system and to a simple Au layer. From the evolution of the magneto-optical properties of Fig. 6, it is deduced that the magnetic modulation ($2\Delta k$) increases with the Co NPs concentration (from 2.2 to $7.5 \times 10^{-5}\,\mu m^{-1}$ at 700 nm). This finally results in the desired increase of the figure of merit $2|\Delta k|L$ with the Co concentration with an improvement of the Au properties for magnetoplasmonics (the modulation of the SPP wavevector in Au is so small that it is not possible to measure it). However, despite such increase due to the Co NPs deposition, the figure of merit for this Au:Co_{NPs} set is still four times smaller than that of a Au/Co/Au trilayer[33] (for this calculations the Au:Co_{NPs} system has been considered on top of a 160 nm Au layer, since the original system was too thin). For the other system, the Co:Au_{NPs} layers, the SPP propagation distance L decreases as the Au NPs concentration increases (from 1.13 to $0.65\,\mu m$ at 700 nm). This unusual behavior is a consequence of the reduction in the contribution of the free electrons to the dielectric constant of the Au NPs, as shown in Fig. 4. Hence, although the imaginary part of the optical constants (related to the absorption of the system) decrease with increasing Au NPs concentration, as the real part of the optical constant becomes also less negative ("less metallic"), it finally results in a reduction of the propagation distance of the plasmon as the Au NPs concentration increases. The magnetic modulation of the plasmon wavevector, $2\Delta k$, increases with the Au NPs concentration (from 0.011 to $0.016\,\mu m^{-1}$ at 700 nm). This also happens for the figure of merit $2|\Delta k|L$ that is larger than that of a Au/Co/Au trilayer, although it is very similar, to that of pure Co. Such increase of the figure of merit is partially hidden by the decay of the propagation distance that could be an important drawback.

IV. SUMMARY

In summary, two complementary systems consisting of a metallic matrix (Au or Co) with embedded metallic NPs (Co or Au) have been studied. The evolution of the optical properties of these systems with the NPs concentration points to an effective optical diameter of the NPs larger than the one obtained by morphological characterisation, due to interface effects. Such effect is especially relevant for the Co:Au_{NPs} system, since its optical properties strongly suggest that the dielectric constants of the Au NPs are different from those of bulk material. These changes can be attributed to a reduction of the free electron contribution to the dielectric constant of Au. Moreover, the non-diagonal component of the dielectric tensor of both systems also suggest that around the NPs there is an effective region that has a MO activity opposite in sign to that of the ferromagnetic material. Regarding the magnetoplasmonic behavior, the figure of merit that combines the magnetic modulation and the propagation distance of the Au:Co_{NPs} layers is smaller than those of the Co:Au_{NPs} set, and it increases considerably with the Co NPs concentration, which is the desired effect. The figure of merit of the Co:Au_{NPs} layers also increases with the Au NPs concentration, however, there is a corresponding reduction of the propagating distance of the SPP (L) due to the different optical properties of the Au NPs regarding those of Au bulk, which could worsen the results of a pure Co layer.

ACKNOWLEDGMENTS

The authors gratefully acknowledge F. J. Palomares and J. M. González from ICMM-CSIC for their assistance with magnetic properties and many helpful discussions. This work was supported by the Spanish MINECO under Project Nos. MAT2011-29194-C02 (MAPS), CSD2007-00041 (NANOSELECT), and CSD2008-00023 (FUNCOAT).

[1]J. Homola, "On the sensitivity of surface plasmon resonance sensors with spectral interrogation," Sens. Actuators, B **41**, 207–211 (1997).
[2]M. Hu *et al.*, "Gold nanostructures: engineering their plasmonic properties for biomedical applications," Chem. Soc. Rev. **35**, 1084–1094 (2006).
[3]R. Zia, J. A. Schuller, A. Chandran, and M. L. Brongersma, "Plasmonics: the next chip-scale technology," Mater. Today **9**, 20–27 (2006).
[4]R. F. Wallis, J. J. Brion, E. Burstein, and A. Hartstein, "Theory of surface polaritons in anisotropic dielectric media with application to surface magnetoplasmons in semiconductors," Phys. Rev. B **9**, 3424–3437 (1974).
[5]H. Feil and C. Haas, "Magneto-optical Kerr effect, enhanced by the plasma resonance of charge carriers," Phys. Rev. Lett. **58**, 65–68 (1987).
[6]G. Armelles, A. Cebollada, A. García-Martín, and M. U. González, "Magnetoplasmonics: Combining magnetic and plasmonic functionalities," Adv. Opt. Mater. **1**, 10–35 (2013).
[7]G. Armelles and A. Dmitriev, "Focus on magnetoplasmonics," New J. Phys. **16**, 045012 (2014).
[8]B. Sepúlveda, A. Calle, L. M. Lechuga, and G. Armelles, "Highly sensitive detection of biomolecules with the magneto-optic surface-plasmon-resonance sensor," Opt. Lett. **31**, 1085–1087 (2006).
[9]V. V. Temnov *et al.*, "Active magneto-plasmonics in hybrid metal–ferromagnet structures," Nat. Photonics **4**, 107–111 (2010).
[10]E. Ferreiro-Vila *et al.*, "Intertwined magneto-optical and plasmonic effects in Ag/Co/Ag layered structures," Phys. Rev. B **80**, 125132 (2009).
[11]D. Regatos *et al.*, "Au/Fe/Au multilayer transducers for magneto-optic surface plasmon resonance sensing," J. Appl. Phys. **108**, 054502 (2010).
[12]C. Hermann *et al.*, "Surface-enhanced magneto-optics in metallic multilayer films," Phys. Rev. B **64**, 235422 (2001).
[13]K. Yang, C. Clavero, J. R. Skuza, M. Varela, and R. A. Lukaszew, "Surface plasmon resonance and magneto-optical enhancement on Au–Co nanocomposite thin films," J. Appl. Phys. **107**, 103924 (2010).
[14]M. Pohl *et al.*, "Tuning of the transverse magneto-optical Kerr effect in magneto-plasmonic crystals," New J. Phys. **15**, 075024 (2013).
[15]A. V. Baryshev, H. Uchida, and M. Inoue, "Peculiarities of plasmon-modified magneto-optical response of gold–garnet structures," J. Opt. Soc. Am. B **30**, 2371–2376 (2013).
[16]G. A. Wurtz *et al.*, "Controlling optical transmission through magneto-plasmonic crystals with an external magnetic field," New J. Phys. **10**, 105012 (2008).
[17]V. I. Belotelov *et al.*, "Enhanced magneto-optical effects in magnetoplasmonic crystals," Nat. Nanotechnol. **6**, 370–376 (2011).
[18]J. Y. Chin *et al.*, "Nonreciprocal plasmonics enables giant enhancement of thin-film Faraday rotation," Nat. Commun. **4**, 1599 (2013).
[19]C. Clavero *et al.*, "Interface effects in the magneto-optical properties of Co nanoparticles in dielectric matrix," Appl. Phys. Lett. **90**, 182506 (2007).

[20]R. Fermento *et al.*, "Optical and magneto-optical properties of Co–SiOx thin films," J. Nanopart. Res. **13**, 2653–2659 (2011).
[21]L. Wang *et al.*, "Plasmonics and enhanced magneto-optics in core–shell Co–Ag nanoparticles," Nano Lett. **11**, 1237–1240 (2011).
[22]J. B. González-Díaz *et al.*, "Plasmonic Au/Co/Au nanosandwiches with enhanced magneto-optical activity," Small **4**, 202–205 (2008).
[23]M. Díaz *et al.*, "Morphological, structural, and magnetic properties of Co nanoparticles in a silicon oxide matrix," J. Nanopart. Res. **13**, 5321–5333 (2011).
[24]M. Ruano *et al.*, "Matrix and interaction effects on the magnetic properties of Co nanoparticles embedded in gold and vanadium," Phys. Chem. Chem. Phys. **15**, 316–329 (2013).
[25]See www.next-tip.com for the description of the different tips commercialized by the company.
[26]J. C. M. Garnett, "Colours in metal glasses and in metallic films," Philos. Trans. R. Soc. London, Ser. A **203**, 385–420 (1904).
[27]O. Levy and D. Stroud, "Maxwell Garnett theory for mixtures of anisotropic inclusions: Application to conducting polymers," Phys. Rev. B **56**, 8035–8046 (1997).
[28]C.-Y. You, S.-C. Shin, and S.-Y. Kim, "Modified effective-medium theory for magneto-optical spectra of magnetic materials," Phys. Rev. B **55**, 5953–5958 (1997).
[29]C. Clavero *et al.*, "Morphology and capping effects in the magnetic and magneto-optical properties of nanoparticulate Co films," Phys. Rev. B **77**, 094417 (2008).
[30]G. Hodes, "When small is different: Some recent advances in concepts and applications of nanoscale phenomena," Adv. Mater. **19**, 639–655 (2007).
[31]M. A. Ordal, R. J. Bell, R. W. Alexander, L. L. Long, and M. R. Querry, "Optical properties of fourteen metals in the infrared and far infrared: Al, Co, Cu, Au, Fe, Pb, Mo, Ni, Pd, Pt, Ag, Ti, V, and W," Appl. Opt. **24**, 4493–4499 (1985).
[32]J. Hamrle *et al.*, "Magneto-optical properties of ferromagnetic/nonferromagnetic interfaces: Application to Co/Au(111)," Phys. Rev. B **64**, 155405 (2001).
[33]D. Martín-Becerra *et al.*, "Enhancement of the magnetic modulation of surface plasmon polaritons in Au/Co/Au films," Appl. Phys. Lett. **97**, 183114 (2010).